Photodissociation dynamics of the NO dimer. I. Theoretical overview of the ultraviolet singlet excited states

Sergey V. Levchenko, Hanna Reisler, and Anna I. Krylov[a),b)]
Department of Chemistry, University of Southern California, Los Angeles, California 90089-0482

Oliver Gessner and Albert Stolow
Steacie Institute for Molecular Sciences, National Research Council Canada, Ottawa, Ontario K1A 0R6, Canada

Huancong Shi and Allan L. L. East[a),c)]
Department of Chemistry and Biochemistry, University of Regina, Regina, Saskatchewan S4S 0A2, Canada

(Received 28 February 2006; accepted 19 June 2006; published online 22 August 2006)

Molecular orbital theory and calculations are used to describe the ultraviolet singlet excited states of NO dimer. Qualitatively, we derive and catalog the dimer states by correlating them with monomer states, and provide illustrative complete active space self-consistent field calculations. Quantitatively, we provide computational estimates of vertical transition energies and absorption intensities with multireference configuration interaction and equations-of-motion coupled-cluster methods, and examine an important avoided crossing between a Rydberg and a valence state along the intermonomer and intramonomer stretching coordinates. The calculations are challenging, due to the high density of electronic states of various types (valence and Rydberg, excimer and charge transfer) in the 6–8 eV region, and the multiconfigurational nature of the ground state. We have identified a bright charge-transfer (charge-resonance) state as responsible for the broadband seen in UV absorption experiments. We also use our results to facilitate the interpretation of UV photodissociation experiments, including the time-resolved 6 eV photodissociation experiments to be presented in the next two papers of this series. © *2006 American Institute of Physics*. [DOI: 10.1063/1.2222355]

I. INTRODUCTION

Experimental studies of the fascinating nitric oxide dimer, $(NO)_2$, continue to shed light on its complex photophysics. Most recently,[1–3] detailed femtosecond time-resolved ultraviolet photodissociation experiments revealed new insights into the dynamics. Motivated by this work, we set out on a theoretical and computational investigation of the UV electronic states of this dimer, with three main goals: (i) to classify and catalog the UV singlet states, (ii) to predict vertical excitation energies and intensities in hopes of identifying likely initial photoabsorbing states, and (iii) to assist in the interpretation of experimental data, particularly in the next two papers of this series [hereafter called II (Ref. 2) and III (Ref. 3)] which investigate the 6 eV photodissociation mechanism. A Communication summarizing the essential results recently appeared in print.[1]

In the ground state, this dimer has a unique binding energy of 700 ± 10 cm^{-1} or 1.99 kcal mol^{-1},[4–6] which is weaker than most hydrogen bonds (5 kcal mol^{-1}), but stronger than bonds typical of van der Waals dimers. Its ground state geometry is a *cis*-ONNO C_{2v}-symmetry trapezoid, with $R(\mathrm{N-O})=1.1515(3)$ Å, $R(\mathrm{N-N})=2.2630(12)$ Å, and $\theta_{\mathrm{NNO}}=97.17(5)°$.[7] The low binding energy, together with strong vibrational and electronic chromophore character, leads to predissociative effects in the infrared and ultraviolet.

The electronic structure of $(NO)_2$ is complex. The loose coupling of two molecular radicals with singly occupied π^* orbitals explains the weak covalent bonding and results in unusual electronic states. Seven infrared excited states arise from the loose coupling of the $^2\Pi$ monomers, and while this coupling has observable influence on rotational[8] and vibrational[9] spectra, the states were correctly characterized and located computationally only in 1998.[10] The multiconfigurational nature of these states poses a challenge for molecular orbital based methods, and two later methodological studies used these 1998 $(NO)_2$ results as benchmarks.[11,12] However, the ultraviolet electronic states have never been properly characterized and this is a central goal of this paper.

As will be discussed in Papers II and III, several experimental techniques have been applied to the investigation of the UV dissociation of the NO dimer. Extensive nanosecond laser photoelectron and photoion imaging studies of the photodissociation dynamics shed details on the dynamics and the product state distributions, suggesting that the dissociation occurred from a planar geometry and exhibits restricted intramolecular vibrational energy redistributions (IVRs) during the dissociation.[6,13–16] The first femtosecond study, in 1998, employed time-resolved photoelectron spectroscopy (TRPES), using 210 nm excitation and 287 nm probe laser wavelengths.[17] TRPES is a method that is sensitive to both charge and energy flow in excited molecules.[18] This TRPES

[a)]Authors to whom correspondence should be addressed.
[b)]Electronic mail: krylov@usc.edu
[c)]Electronic mail: allan.east@uregina.ca

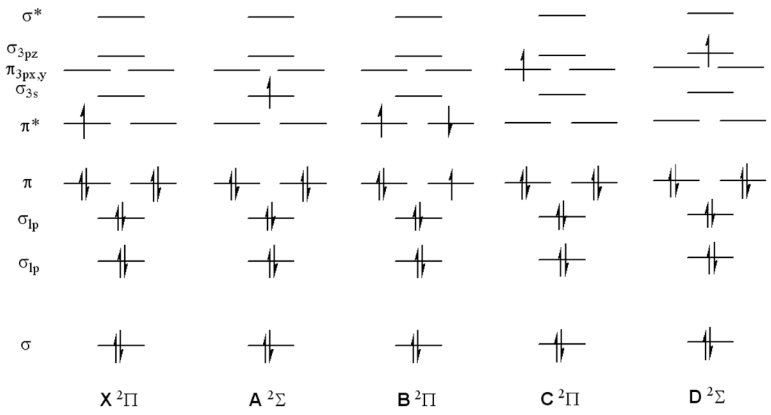

FIG. 1. Leading electron configurations for the lowest five doublet states of the NO monomer. Note that other electronic states arise from a $\pi^3\pi^{*2}$ configuration other than the $B\ ^2\Pi$, namely, $a\ ^4\Pi$, $L\ ^2\Phi$, and two other $^2\Pi$ states.

study proposed that $(NO)_2$ dissociation dynamics at 210 nm was not direct but stepwise, via nonadiabatic interactions involving an intermediate state. Using single exponential fits, the decay rate of the dimer parent ion appeared to be incommensurate with the rise of the free NO(A) products. Hence, it was proposed that there was an intermediate "dark state" which had unfavorable ionization correlations for producing the ground state of the dimer cation. An alternative hypothesis arose in 2003, when a TRPES study using photoelectron and photoion imaging but with a different pump wavelength (200.5 nm) was presented,[19] followed by experiments over a range of pump laser wavelengths (200–235 nm).[20] Based upon single exponential fits, it was argued that a one-step process from an initially excited valence state to a dissociative dimer 3s Rydberg state was sufficient to explain their data, with no need to invoke any intermediate step.

In Paper II, a new high-resolution TRPES study at 5.9 eV pump energy demonstrates that the dissociation dynamics cannot be modeled by single exponential kinetics. Rather, it is fitted with very high accuracy by a two-step sequential model involving an uncharacterized intermediate configuration. In Paper III, a time-resolved coincidence imaging spectroscopy (TRCIS) study demonstrates that this intermediate configuration is inconsistent with a dimer 3s Rydberg state but is consistent with a dimer $3p_y$ Rydberg state that evolves to free NO(A)+NO(X) products. The theoretical predictions to be presented here played a vital role in the state assignments and mechanisms to be presented in Papers II and III.

This paper is organized as follows. In Sec. II we present the state catalog, using excimer theory to classify the dimer states via correlation to monomer states. In Sec. III we discuss the computational methods used to investigate the states. In Sec. IV we present our results, in three subsections. In Sec. V we discuss the interesting theoretical aspects of the computational results, followed by the application of our results to the elucidation of experimental observations. Finally, in Sec. VI we provide a short summary of the highlights.

II. THEORY

A. NO monomer orbitals and states

The electronic states of weakly bound dimers are best understood by relating them to the states of the separated monomers. The lowest-energy singlet states of the dimer arise from combining a ground state $X\ ^2\Pi$ monomer with a monomer in any of its lowest five doublet states. Figure 1 shows the electronic configurations of these five states. The Rydberg states (A, C, and D) prefer *shortened* R(N–O) bond lengths, because an electron is excited from an *antibonding* orbital to a Rydberg one ($\pi^* \rightarrow$ Ryd). The B state, a $\pi \rightarrow \pi^*$ state, prefers a longer R(N–O) bond length. The B and C states, both of $^2\Pi$ symmetry, exhibit an avoided crossing at an R(N–O) distance quite near that of the ground state equilibrium bond length.[21]

As will be shown, many singlet states of the dimer arise from combining a ground state cation, $X\ ^1\Sigma\ NO^+$, with a variety of hypothetical (possibly metastable) electronic states of NO^-. NO^- has a low and debated ionization potential and perhaps no bound singlet electronic states,[22,23] but in the presence of an approaching NO^+ monomer some of its hypothetical states could become bound. For instance, Rydberg states of a monomer anion, while seemingly absurd and surely unstable, will theoretically correlate to Rydberg states of a neutral dimer, some of which may be bound states.

B. NO dimer orbital symmetries

Our symmetry axis convention, adopted in Papers II, III, and Ref. 1, has x as the out-of-plane axis, y as the intermonomer axis, and z as the axis of the dipole moment (Fig. 2). Our use of C_{2v} symmetry labels assumes that a b_2-symmetry orbital preserves its phase when subjected to a σ_{yz} mirror plane, i.e., the plane containing all nuclei.

Figure 3 displays an orbital energy chart, showing the orbitals of interest (ignoring the lowest five a_1 and five b_2 occupied orbitals, i.e., those derived from monomers' core and σ-space orbitals). Four orbitals, denoted $6a_1$, $1b_1$, $6b_2$, and $1a_2$, arise from combinations of each monomer's doubly

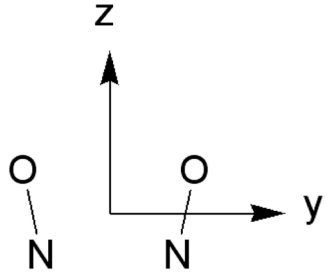

FIG. 2. The axis convention.

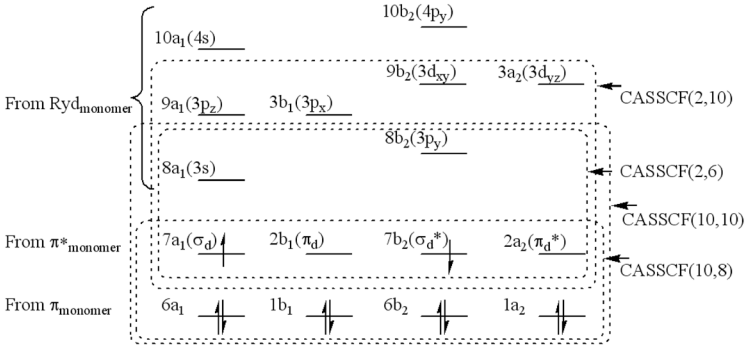

FIG. 3. $(NO)_2$ orbital notations and CASSCF active spaces. The horizontal lines represent orbitals. The electron configuration shown is one of the two spin components of the dominatingly bright charge-transfer state CT_1. Alternative dimer labels are in parentheses, e.g., the $7a_1$ orbital is a σ-type dimer-bonding orbital (hence σ_d) arising from constructive overlap of two in-plane $\pi^*_{monomer}$ orbitals.

degenerate π orbitals. Four more arise from combinations of the π^* orbitals, and we use an alternative "dimer notation" for these[10] (in parentheses in Fig. 3) that indicates the type of bonding or antibonding character *between the monomers* these orbitals have. Finally, the eight dimer Rydberg orbitals that should arise from the $3s_{monomer}$ and $3p_{monomer}$ orbitals are also shown in Fig. 3, and we also provide the label of the resulting dimer Rydberg orbital in each case. Of particular importance to the $X+A$ states, the $8a_1$ and $8b_2$ dimer orbitals are the $3s$ and $3p_y$ dimer Rydberg orbitals, which primarily arise from plus-and-minus combinations of the $3s_{monomer}$ Rydberg orbitals as mentioned previously.[1] Orbital orderings, even within symmetry blocks, can vary across the potential energy surface, which gives rise to computational challenges and must be carefully monitored.

C. NO dimer state catalog

Excimer theory provides a convenient way to label the ultraviolet states of a weakly bound dimer. East and Lim provided a molecular orbital (MO) description of excimer theory, and used it to label a variety of states of naphthalene dimer.[24] As described there, the interaction of a single-photon excited monomer with a ground state monomer leads to two ER (excimer, exciton-resonance) states, σ and γ, with two associated CT (charge-transfer, charge-resonance) states, called δ and ρ,

$$|\sigma\rangle = 2^{-1/2}(A^*B - AB^*),$$

$$|\gamma\rangle = 2^{-1/2}(A^*B + AB^*),$$

$$|\delta\rangle = 2^{-1/2}(A^-B^+ + A^+B^-),$$

$$|\rho\rangle = 2^{-1/2}(A^-B^+ - A^+B^-). \quad (1)$$

In this notation, A^* is an excited state of monomer A involving excitation of an electron from occupied orbital i to a previously unoccupied orbital a, A^+ is the cation resulting from removal of an electron from orbital i, and A^- is the anion resulting from addition of an electron to orbital a.

Although that description corresponded to the usual case of closed-shell monomers with nondegenrate highest occupied molecular orbitals (HOMOs) and lowest unoccupied molecular orbitals (LUMOs), the result is similar for our NO dimer case of open-shell monomers and degenerate pairs of HOMOs and LUMOs. The interaction of one spatial component of the degenerate doublet ground state with one of a doublet excited state will lead to a set of four singlet states, denoted $\{^1\sigma, ^1\gamma, ^1\delta, ^1\rho\}$, and a set of four triplet states, denoted $\{^3\sigma, ^3\gamma, ^3\delta, ^3\rho\}$. Hence, combining an $X\,^2\Pi$ monomer (two spatial components, call them x and y) with an $A\,^2\Sigma$ monomer (one spatial component) will give rise to eight singlets $\{^1\sigma_x, ^1\sigma_y, ^1\gamma_x, ^1\gamma_y, ^1\delta_x, ^1\delta_y, ^1\rho_x, ^1\rho_y\}$ and eight triplets. The focus of this study is on singlet dimer states only.

In Table I we present the catalog of dimer states, and their corresponding irreducible representations in C_{2v} symmetry, which arise from the $X+A$, $X+B$, $X+C$, and $X+D$ monomer combinations. The states arising from $X+X$ are included for completeness, although excimer theory does not straightforwardly apply to them. Note that the CT states do not correlate to neutral monomers as suggested by $X+A$ notation, but to $NO^+ + NO^-$ asymptotes, which are higher in energy.

III. COMPUTATIONAL METHODS

Several complementary methods were employed. Multireference calculations, using the MOLPRO 2002 code,[26] included the complete active space self-consistent field[27,28] (CASSCF) and internally contracted multireference configuration interaction singles and doubles[29,30] (MRCISD) methods. Single-reference equations-of-motion coupled-cluster (EOM-CC) calculations, using the Q-CHEM (Ref. 31) and ACES II (Ref. 32) codes, included the traditional implementation (EOM-CCSD for excitation energies, or EOM-EE-CCSD),[33] its spin-flip version (EOM-SF-CCSD),[34] and the EOM-EE method including triple excitations in the EOM part, EOM-EE-(2,3).[35,36] The CASSCF calculations were useful for qualitative calculations, while the high-level MRCI and EOM-CC methods were used for more quantitative work.

In the CASSCF runs, the evenly weighted state-averaged algorithm was used, with particular active spaces chosen for particular groups of states, as this was often the only way to achieve convergence. It also provides a convenient way of computing transition dipole moments, due to the use of a common molecular-orbital set for multiple states. Attempts to include more than 22 states in a state-averaging run were thwarted by a limitation of the print algorithm, although computational cost would have also become a concern. MRCISD runs employed CASSCF reference spaces, orbitals from state-averaged CASSCF runs, and froze four core

TABLE I. The singlet states of NO dimer that arise from the five lowest monomer states, derived from excimer theory.

Monomer asymptote	Asymptote energy (T_e)[a] (eV)	ER state label	CT state label	Symmetry of both states	Dominant configurations[b,c]
$X\,^2\Pi+D\,^2\Sigma$	6.582	$^1\gamma_x$	$^1\delta_x$	A_2	$2b_19b_2\pm2a_29a_1$
		$^1\gamma_y$	$^1\delta_y$	B_2	$7a_19b_2\pm7b_29a_1$
		$^1\sigma_x$	$^1\rho_x$	B_1	$2b_19a_1\pm2a_29b_2$
		$^1\sigma_y$	$^1\rho_y$	A_1	$7a_19a_1\pm7b_29b_2$
$X\,^2\Pi+C\,^2\Pi$	6.463	$^1\gamma_{xx}$	$^1\delta_{xx}$	B_2	$2b_13a_2\pm2a_23b_1$
		$^1\gamma_{xy}$	$^1\delta_{xy}$	A_2	$2b_110b_2\pm2a_210a_1$
		$^1\gamma_{yx}$	$^1\delta_{yx}$	A_2	$7a_13a_2\pm7b_23b_1$
		$^1\gamma_{yy}$	$^1\delta_{yy}$	B_2	$7a_110b_2\pm7b_210a_1$
		$^1\delta_{xx}$	$^1\rho_{xx}$	A_1	$2b_13b_1\pm2a_23a_2$
		$^1\sigma_{xy}$	$^1\rho_{xy}$	B_1	$2b_110a_1\pm2a_210b_2$
		$^1\sigma_{yx}$	$^1\rho_{yx}$	B_1	$7a_13b_1\pm7b_23a_2$
		$^1\sigma_{yy}$	$^1\rho_{yy}$	A_1	$7a_110a_1\pm7b_210b_2$
$X\,^2\Pi+B\,^2\Pi$	5.693	$^1\gamma_{xx}$	$^1\delta_{xx}$	B_2	Lengthy combinations: $\pi^7\pi^{*3}$
		$^1\gamma_{xy}$	$^1\delta_{xy}$	A_2	
		$^1\gamma_{yx}$	$^1\delta_{yx}$	A_2	
		$^1\gamma_{yy}$	$^1\delta_{yy}$	B_2	
		$^1\sigma_{xx}$	$^1\rho_{xx}$	A_1	
		$^1\sigma_{xy}$	$^1\rho_{xy}$	B_1	
		$^1\sigma_{yx}$	$^1\rho_{yx}$	B_1	
		$^1\sigma_{yy}$	$^1\rho_{yy}$	A_1	
$X\,^2\Pi+A\,^2\Sigma$	5.451	$^1\gamma_x$	$^1\delta_x$	A_2	$2b_18b_2\pm2a_28a_1$
		$^1\gamma_y$	$^1\delta_y$	B_2	$7a_18b_2\pm7b_28a_1$
		$^1\sigma_x$	$^1\rho_x$	B_1	$2b_18a_1\pm2a_28b_2$
		$^1\sigma_y$	$^1\rho_y$	A_1	$7a_18a_1\pm7b_28b_2$
$X\,^2\Pi+X\,^2\Pi$	0		CT_1	B_2	$7a_17b_2$
			CT_2	B_2	$2b_12a_2$
		IR_3	CT_3	A_2	$7a_12a_2\pm2b_17b_2$
		IR_2	CT_4	A_1	$2b_12b_1\pm2a_22a_2$
		IR_1	CT_5	B_1	$7a_12b_1\pm2a_27b_2$
		X	CT_6	A_1	$7a_17a_1\pm7b_27b_2$

[a]From Huber and Herzberg (Ref. 25)
[b]The orbitals singly occupied by the two highest-energy electrons. The remaining 28 electrons fill 14 orbitals, up to $6a_1^21b_1^26b_2^21a_2^2$.
[c]The ninth and tenth orbitals of a_1 and b_2 symmetries may have mixed character at dimer distances, and are difficult to ascribe solely to $X+D$ or $X+C$ individually.

orbitals, although we point out that exploratory runs with ten frozen orbitals (core+sigma space) had only minor differences upon relative state energies. Our largest MRCISD used approximately 74×10^6 configurations.

The EOM-EE-CCSD method accurately describes singly excited electronic states, even in the cases when the reference wave function has considerable multiconfigurational character;[37] however, states with doubly excited character would appear artificially high in energy.[12,37] Some of the dark diabatic $(NO)_2$ states near 6 eV are formally double excitations with respect to any reference configuration, whether it be σ_d^2 (EE version) or $\sigma_d^1\sigma_d^{*1}$ (SF version), and hence will be described poorly and placed too high in energy. The bright states, however, should not suffer in this manner. EOM-CCSD has the attractive feature of treating interacting states of different nature (e.g., Rydberg and valence) on the same footing, which is important for the UV states of this dimer. States were analyzed using the EOM-CCSD amplitudes, transition dipoles, and the natural bond-orbital (NBO) analysis[38] of the excited states' one-electron density.

Basis sets used with the CASSCF and MRCISD calculations were Dunning based. Our VTZ+*R* label denotes aug-cc-pVTZ, which has one diffuse set of *s*, *p*, *d*, and *f* functions (overall contracted set $5s4p3d2f$).[39] Our VTZ+2*R* label denotes a modified aug-cc-pVTZ set in which the diffuse *s* and *p* sets were replaced with two *s* and two *p* sets (overall contracted set $6s5p3d2f$), chosen via even-tempering based on the ratio of the two most diffuse exponents in the cc-pVTZ set. In the EOM-EE-CCSD and EOM-SF-CCSD calculations, we employed the 6-311(2+)G($2df$) basis set, derived from the Pople split-valence triple-zeta polarized basis set 6-311G($2df$) (Ref. 40) augmented with two sets of diffuse *s* and *p* functions. In the EOM-EE(2,3) calculations, the 6-31+G* basis set[41] is used. All basis sets used

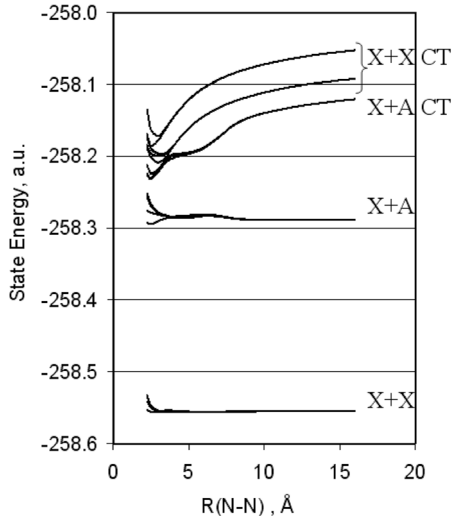

FIG. 4. CASSCF(2,6)/VTZ+R energies of several states of NO dimer vs intermonomer distance.

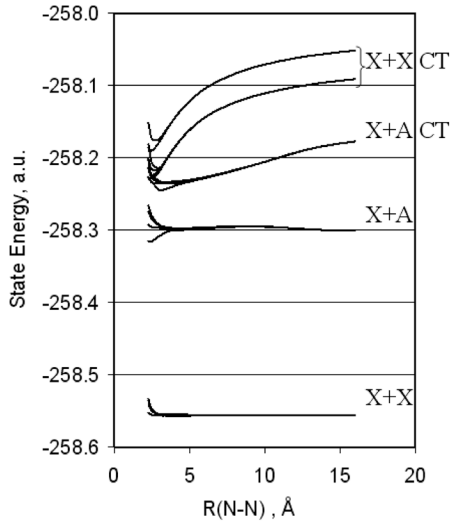

FIG. 5. CASSCF(2,6)/VTZ+2R energies of several states of NO dimer vs intermonomer distance.

pure spherical harmonic sets for d and f functions, except the 6-31+G* set, which employed a set of six Cartesian d functions per atom.

Absorption intensity refers to the square of the electronic transition dipole moment, $\langle\mu\rangle^2=\langle\Psi_i|\mu|\Psi_0\rangle\langle\Psi_0|\mu|\Psi_i\rangle$. Nonrelaxed EOM intensities and other excited state properties were calculated using the EOM-CC properties code implemented in Q-CHEM.[31]

IV. RESULTS

A. State energies versus intermonomer distance

As a qualitative demonstration of the state correlations between dimer and monomer in Table I, we performed state-averaged CASSCF single-point calculations for many dimer states, at the experimental ground state geometry[7] and then for 23 other choices of intermonomer distance up to 16 Å. To elucidate the effect of a second set of diffuse functions, each calculation was done twice, with VTZ+R and VTZ+2R bases.

Figures 4 and 5 summarize the data from 18-state-averaged CASSCF(2,6) runs, where the active space consists of the four π^*_{monomer} orbitals and the two Rydberg a_1 and b_2 orbitals arising from the monomers 3s orbitals (see Fig. 3). The resulting 36 Slater determinants give rise to 21 singlet states (eight A_1, four B_1, five B_2, and four A_2). The three states having two Rydberg electrons were ignored, and the remaining 18 were equally weighted in the state averaging. The 18 state energies are plotted in Figs. 4 and 5; they contain all states arising from $X+X$, $X+A$, CT($X+A$), and CT($X+X$).

Figure 4, from the VTZ+R basis set, features some artificial bulges near 7–8 Å for the $X+A$ and CT($X+A$) states. When an additional set of s and p diffuse functions is added to the basis set (Fig. 5), the bulges are far less pronounced and occur at further distances (11–13 Å). Going from VTZ+R to VTZ+2R also resulted in a further energy lowering of the CT($X+A$) energies for large intermonomer separations, because it allows the electron to get further away; remember that the asymptote leads to a fictitious Rydberg state of NO anion, and hence really leads to $NO^+ + NO + e^-$.

There is a fundamental qualitative problem with the computed CT($X+X$) states at large intermonomer separation, because of computational difficulties associated with the anion product, NO^-. The true electron affinity of NO is debated;[22,23] the best calculations suggest a very small value (0.03 eV), likely for a triplet ground state. Hence, *all* singlet states of the anion are likely to be unstable with respect to e^- detachment, and thus *all* charge transfer states of the dimer in Figs. 4 and 5 would truly dissociate to the same asymptotic energy ($NO^+ + NO + e^-$). However, the calculations of CT($X+X$) singlet states have instead locked onto the higher-energy metastable anionic states. Furthermore, the CASSCF energies of these states at all intermonomer distances are overpredicted, based on our later comparisons to MRCISD and EOM-CC vertical excitation energies.

Figure 6 presents a more complete picture, containing more states. It was derived from Fig. 5 by adding two other sets of CASSCF data that targeted the $X+B$ and $X+C$ states. The $X+B$ data come from CASSCF(10,8)/VTZ+R runs, state averaged over 12 states (four $X+X$ and eight $X+B$). The $X+C$ data come from CASSCF(2,10)/VTZ+2R runs, state averaged over 20 states [four $X+X$, four $X+A$, eight $X+C$, and four CT($X+A$)]. See Fig. 3 for the active space descriptions.

The lower left-hand region, i.e., 5–7 eV, R(N–N) = 1.9–2.5 Å, was studied more quantitatively with EOM-EE-CCSD calculations. The resulting potential energy curves for four singly excited states are presented in Fig. 7. The leading character of the states at the ground state equilibrium geometry is shown on the right side of the figure. The first important observation is the lowering of state energies, particularly the $^1B_2(\text{CT}_1, X+X)$ state whose vertical excitation energy dropped from 9.6 (CASSCF, Fig. 6) to 6.1 eV. The $^1A_1(3p_z, X+D)$ state comes from the higher $X+D$ manifold that was not considered for Fig. 6. A second important observation is the preference for R(N–N)=2.1–2.3 Å for all four states with EOM-EE-CCSD, clearly not seen in the

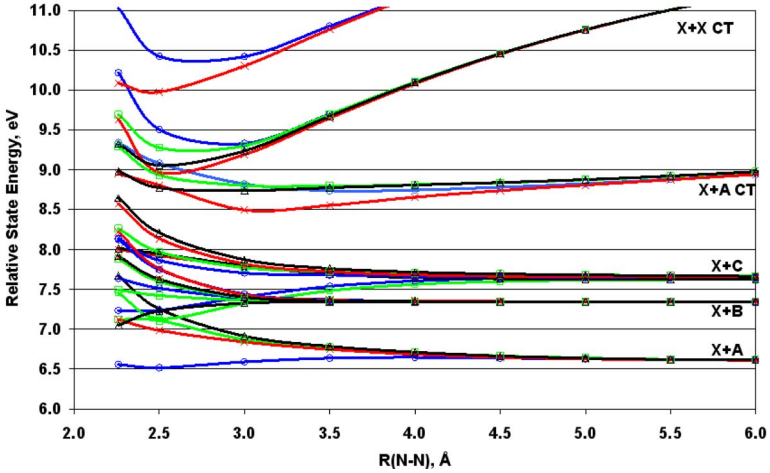

FIG. 6. CASSCF potential energy curves for the complete sets of UV excited singlet states of $(NO)_2$, vs intermonomer distance. Results were taken from various state-averaged runs; see text. Not shown are states of higher multiplicity, and states correlating with higher excited states of the monomer (e.g., $X+D$, $X+E$, etc.). The states are color coded by symmetry: A_1 (blue), B_1 (green), B_2 (red), and A_2 (black). Note that CASSCF places the $X+X$ CT states too high, relative to the excimer (ER) states.

CASSCF data. Note that other states, e.g., $^1B_2(\mathrm{CT}_2, X+X)$ and $^1B_2(^1\delta_y, X+A)$, might exist in this Fig. 7 region but could not be properly considered within the EOM-EE-CCSD formalism. The presented EOM-EE-CCSD relative energies are significantly more reliable than the CASSCF ones.

The lower energy of the CT state in EOM-EE-CCSD does allow the observation of adiabatic mixing and an avoided crossing of the two $^1B_2$ states in Fig. 7. The diabatic Rydberg $(3p_y)$ and valence CT $(\sigma_d \rightarrow \sigma_d^*)$ states are found to be strongly mixed at the ground state geometry, with the mixing depending strongly on the N–N distance. This is vividly demonstrated by the dependence of the absorption intensity on the intermonomer distance, shown in Fig. 8. The decrease in intensity of the lower energy adiabatic state at short N–N bond is due to the change in its character from the brighter CT state to the Rydberg state,[43] with inverted results for the higher state. The lower state would eventually lose its gained CT character at even longer N–N distances, as the CT diabatic state rises in energy. Note that the location and extent of this avoided crossing are very sensitive to the relative energy of the diabatic states and other degrees of freedom. Thus, Fig. 7 provides only an approximate location of the intersection.

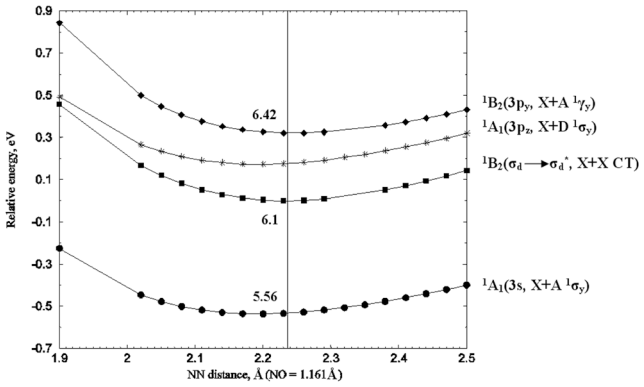

FIG. 7. The EOM-EE-CCSD/6-311(2+)G(2*df*) potential energy curves as a function of the intermonomer distance. The $R(\mathrm{N-O})$ and $\angle\mathrm{ONN}$ values were taken to be 1.161 Å and 99.6° (Ref. 42). The zero of energy corresponds to the minimum of the $^1B_2(\sigma_d \rightarrow \sigma_d^*, X+X\ \mathrm{CT})$ state. Vertical excitation energies are also shown. The characters of the $^1B_2$ states are inverted at smaller N–N distances due to an avoided crossing.

B. Vertical excitation energies and transition moments

Due to the high density of electronic states of different character in the UV region, and the multiconfigurational character of the ground state, $(NO)_2$ offers tough challenges to both EOM-CC and multireference methods. We therefore used both approaches in our search for the probable absorbing states in the UV for this dimer.

Table II presents EOM-EE-CCSD/6-311(2+)G(2*df*) vertical excitation energies and absorption intensities for 18 adiabatic states. This calculation finds substantial intensity only for the two lowest B_2 states. As discussed above (Fig. 8), these two adiabatic states gain their intensity from their charge-transfer CT_1 component, as they consist of unequal admixtures of two main diabatic components: the CT_1 state $(\sigma_d^1 \sigma_d^{*1}$ occupation) and the Rydberg $X+A\ ^1\gamma_y(3p_y)$ state $(\sigma_d^1 3p_y^1$ occupation).

Several CASSCF vertical-excitation calculations were also performed, and they confirmed that the brightest diabatic state by far is the CT_1 state. However, they also demonstrated that the EOM-EE-CCSD calculation, which omits doubly excited diabatic states, may underestimate the number of B_2 states that borrow intensity from CT_1. Table III

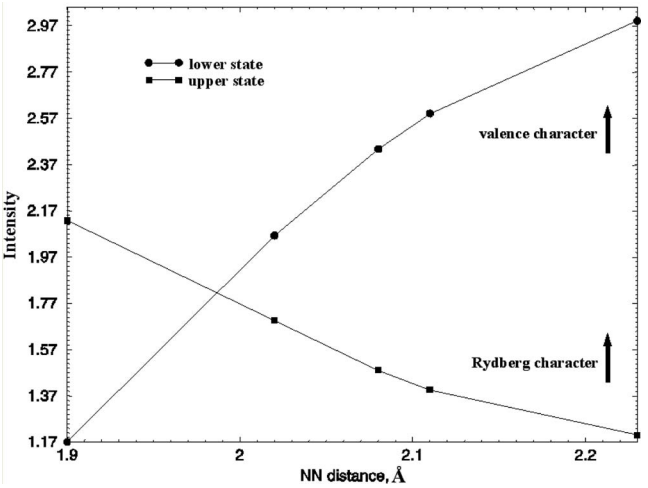

FIG. 8. The dependence of the absorption intensity $\langle \tilde{\mu}_{\mathrm{elec}} \rangle^2$ vs $R(\mathrm{N-N})$ for the two B_2 transitions of mixed Rydberg $(3p_y)$ and valence $(\sigma_d \rightarrow \sigma_d^*)$ character, from the EOM-EE-CCSD runs of Fig. 7.

TABLE II. Vertical excitation energies (eV) and intensities (a.u.), UV singlet states, from EOM-EE-CCSD/6-311(2+)G(2*df*). Computed at older geometry (Ref. 42) R(N–N)=2.236 Å, R(N–O)=1.161 Å, θ(NNO)=99.6°. Single excitations from $7a_1^2$ reference only.

$^1A_1$ states		$^1B_1$ states		$^1B_2$ states		$^1A_2$ states	
E	Intensity	E	Intensity	E	Intensity	E	Intensity
5.56	0.004	6.18	0.017	6.10	3.002	7.20	0
6.27	0.083	7.53	0	6.42	1.196	7.44	0
7.12	0.075	8.01	0	7.38	0.136	8.24	0
7.33	0.0002	8.51	0.070	8.10	0.020	8.50	0
7.80	0.0003			8.28	0.005		

shows results from a nine-state-averaged CASSCF(2,10)/VTZ+2R run, which includes five B_2 states missing from the EOM-CCSD run. The adiabatic state with the largest amount of CT_1 character is artificially high (10.29 eV), a significant failure of this method, but the table demonstrates that CT_1 is, in fact, distributed across *all eight* B_2 states present in the calculation, across a 4 eV range, and that the intensities are closely linked to how much CT_1 character the state contains ($I_i \approx 1.6 c^2_{i,CT_1}$). The CT_2 state produces very little intensity because it is a forbidden two-electron excitation from the ground state.

Table IV contrasts various levels of theory for vertical excitation data to two particular B_2 adiabatic states: the one that is predominantly Rydberg $X+A\ ^1\gamma_y(3p_y)$, and the lowest one whose leading character is valence $X+X$ CT_1. The Rydberg state energy is affected more by basis set than by correlation method, with energies of 6.4–6.9 eV when two diffuse shells are provided, versus 7.0–7.5 eV when only one is provided. $E(CT_1)$, however, strongly depends on correlation method: as the method improves going down the table, this energy falls from 9.7 eV to as low as 6.1 eV.

Note the large variation in intensity predictions in both the Rydberg state and the state that is predominantly CT_1. In each case, the intensity is largely due to how much CT_1 character the state contains, and this varies due to the number of B_2 states considered in each calculation. For example, the CASSCF and MRCI runs based on a (10,10) active space produce lower intensities for the CT_1 state (<0.6 a.u.), due to intensity borrowing of other valence states (such as $X+B$) which do not appear with the smaller (2,6) active space.

The EOM-SF-CCSD method, with a $\sigma_d^1\sigma_d^{*1}$ reference, might describe some of the dimer states better than EOM-EE-CCSD, which uses a σ_d^2 reference and hence omits the minor components of the ground state (σ_d^{*2}) and the $3p_y$ Rydberg state ($\sigma_d^{*1}3p_y^1$). These errors cancel in the computation of the Rydberg excitation energy, and hence the EE and SF predictions agree (6.4 eV). However, the EE estimate of the CT state excitation energy (6.1 eV) might be affected by this problem, and the SF calculation could result in an improved energy. Also note that the EOM-SF description of Rydberg states (or any other states of "nondiradical" $\sigma_d^n\sigma_d^{*2-n}$ character) is plagued by spin contamination,[44] allowing states of another multiplicity to mix. Here, this artificial intensity borrowing erodes the amount of CT_1 character and, consequently, intensity, as seen in Table IV.

Inclusion of triple excitations in the EOM-EE-(2,3) method results in the systematic improvement in accuracy for both singly and doubly excited states. Unfortunately, as it is computationally demanding, we had to reduce the Rydberg basis-function sets from two to one, and, as mentioned above; this resulted in a higher Rydberg-state energy. This artificial rise was alleviated by an extrapolation technique.[45]

C. State energies versus symmetric R(N–O) stretch

From earlier work on the NO monomer,[21] it is known that the Rydberg states A, C, and D prefer short R(N–O) bond lengths (~1.06 Å); a bond order of 3 is predicted by molecular orbital theory. The ground state, with a bond order of 2.5, prefers R(N–O)=1.15 Å. The B state, a $\pi^* \leftarrow \pi$ state, has a bond order of 1.5, and hence prefers a longer bond length (~1.45 Å). Therefore, in ER states of the dimer, we would expect that $X+A$, $X+C$, and $X+D$-based states prefer shorter R(N–O) bond lengths, and $X+B$-based states prefer longer bond length, than $X+X$. The bright $X+X$ CT_1 state of occupation $7a_1^1 7b_2^1(\sigma_d\sigma_d^*)$ would be predicted to have the same R(N–O) preferences as the $X+X$ ER state at bound charge-resonance geometries. From these considerations, we offer Fig. 9 as a crude prediction of R(N–O) effects upon B_2-symmetry state energies.

TABLE III. Vertical excitation energies (eV) and intensities (a.u.), UV $^1B_2$ states, from CASSCF(2,10)-9SA/VTZ+2R. Computed at newer geometry (Ref. 7): R(N–N)=2.2630 Å, R(N–O)=1.1515 Å, θ(NNO)=97.17°. State-averaged calculation, lowest eight B_2 states and ground A_1 state evenly weighted.

State	E	Leading component of wave function[a]	Bright-state component of wave function[a]	Intensity
$X+A\ ^1\gamma_y$ $(3p_y)$	6.89	$0.9481\|7a_1^1 8b_2^1\rangle$	$0.1827\|7a_1^1 7b_2^1\rangle$	0.078
$X+D\ ^1\gamma_y$	7.71	$0.9366\|7a_1^1 9b_2^1\rangle$	$0.2828\|7a_1^1 7b_2^1\rangle$	0.202
$X+C\ ^1\gamma_{xx}$	8.53	$0.7599\|3b_1^1 2a_2^1\rangle$	$0.1321\|7a_1^1 7b_2^1\rangle$	0.048
$X+X$ CT_2	8.92	$0.6916\|2b_1^1 2a_2^1\rangle$	$0.3855\|7a_1^1 7b_2^1\rangle$	0.334
$X+A\ ^1\delta_y$	9.30	$0.9192\|8a_1^1 7b_2^1\rangle$	$0.1305\|7a_1^1 7b_2^1\rangle$	0.019
$X+C\ ^1\delta_{xx}$	9.61	$0.6538\|2b_1^1 3a_2^1\rangle$	$0.4138\|7a_1^1 7b_2^1\rangle$	0.331
$X+D\ ^1\delta_y$	9.81	$0.9680\|9a_1^1 7b_2^1\rangle$	$0.0185\|7a_1^1 7b_2^1\rangle$	0.002
$X+X$ CT_1 $(\sigma_d \rightarrow \sigma_d^*)$	10.29	$0.7295\|7a_1^1 7b_2^1\rangle$	$0.7295\|7a_1^1 7b_2^1\rangle$	0.880

[a]The ket notation $|\phi_1^1\phi_2^1\rangle$ represents $1/\sqrt{2}(|\phi_1\alpha,\phi_2\beta\rangle - |\phi_1\beta,\phi_2\alpha\rangle)$.

TABLE IV. Vertical excitation results for two $^1B_2$ adiabatic states of $(NO)_2$. All computations used the newer geometry (Ref. 7): R(N–N)=2.2630 Å, R(N–O)=1.1515 Å, θ(NNO)=97.17°, except the EOM-EE-(2,3) results which used the older geometry (Ref. 42), R(N–N)=2.236 Å, R(N–O)=1.161 Å, θ(NNO)=99.6°.

	$X+X$ CT$_1$ ($\sigma_d \rightarrow \sigma_a^*$)		$X+A\,^1\gamma_y$ (Ryd $3p_y$)	
Method[a–c]	Leading coefficient[d]	Vertical energy (eV)[e]	Leading coefficient[d]	Vertical energy (eV)[e]
CASSCF(2,6)-6SA/VTZ+R	0.78	9.68(1.2)	0.88	7.47(0.4)
CASSCF(2,6)-6SA/VTZ+2R	0.87	9.63(1.4)	0.96	6.87(0.1)
CASSCF(10,10)-3SA/VTZ+R	0.45	8.53(0.4)	0.86	7.02(0.1)
CASSCF(10,10)-3SA/VTZ+2R	0.51	8.52(0.5)	0.89	6.45(0.0)
MRCISD(2,6)-6SA/VTZ+R	0.74	8.33(1.5)	0.80	7.20(0.5)
MRCISD(2,6)-6SA/VTZ+2R	0.82	8.15(1.8)	0.88	6.75(0.1)
MRCISD(10,10)-3SA/VTZ+R	0.49	7.97(0.6)	0.81	7.04(0.2)
MRCISD(10,10)-3SA/VTZ+2R	0.54	7.88(0.7)	0.84	6.60(0.0)
EOM-EE-CCSD/6-311(2+)G(2df)		6.08(2.4)		6.37(1.8)
EOM-SF-CCSD/6-311(2+)G(2df)		6.87(1.9)		6.39(0.2)
EOM-EE-(2,3)/6-31+G*		6.67		7.52
EOM-EE-(2,3)/extrapolated		6.49		6.75

[a]CASSCF details: (x,y) indicates an active space of x electrons in y orbitals. mSA indicates m states (ground A_1 and $m-1B_2$ states) were included in the state-averaged CASSCF.
[b]MRCISD details: the (x,y) and mSA notation indicates the initial CASSCF parameters. Each MRCISD run used four frozen-core orbitals, and focused on an individual electronic state.
[c]EOM-EE-(2,3) details: These calculations used four frozen-core orbitals. Extrapolated refers to a basis set correction from 6-31+G* to 6-311(2+)G(2df), made by adding the difference between the EOM-EE-CCSD excitation energies calculated at the two basis sets, and assuming that the EOM-EE-(2,3) correction to the ground state energy is the same with either basis set.
[d]The leading coefficient is for the CT$_1$ configuration $1/\sqrt{2}(|7a_1\alpha,7b_2\beta\rangle - |7a_1\beta,7b_2\alpha\rangle)$ in column 2, and for the $3p_y$ Rydberg configuration $1/\sqrt{2}(|7a_1\alpha,8b_2\beta\rangle - |7a_1\beta,8b_2\alpha\rangle)$ in column 4, based on pseudocanonical orbitals.
[e]Absorption intensities in a.u. appear in parentheses where available.

In Fig. 10 we show our EOM-EE-CCSD/6-311(2+)G(2df) results for selected states in the 1.1–1.2 Å region. There is an avoided crossing between the $X+X$ CT and $X+A$ Rydberg B_2 states in this R(N–O) dimension, just as there was in the R(N–N) dimension in Fig. 7. The concomitant switch in intensity of each state versus R(N–O) is seen in Fig. 11, just as we had seen versus R(N–N) in Fig. 8. This avoided crossing was incorporated into the larger sketch of Fig. 9. Note that this crossing is tentatively located at R(N–O)=1.14 Å and E=6 eV, the very region accessed by our 6 eV pump photons in Papers II and III, and that both adiabatic states are sloped towards shorter R(N–O) bond lengths. Hence it is easy to imagine how the initially excited CT state can quickly evolve into a $3p_y$ Rydberg state with vibrational excitation in the ν_1 NO symmetric stretch.

However, we stress that these sketches are only qualitative, and that other Rydberg states from $X+C$ or $X+D$ as-

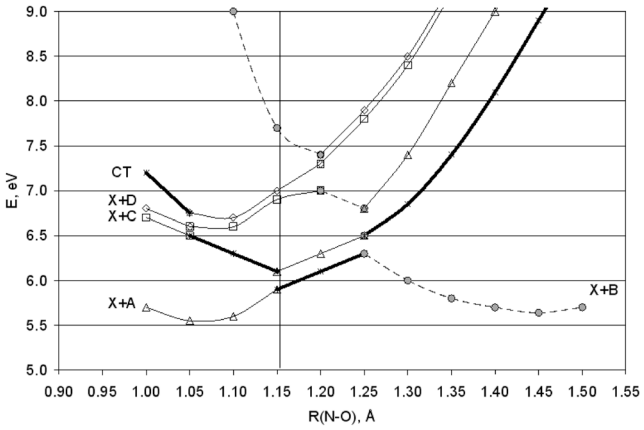

FIG. 9. Sketch of the potential energy surfaces (PESs) of various B_2 dimer states vs symmetric R(N–O) stretch, showing avoided crossings. Points were not calculated, but estimated based on known curves for NO monomer (Ref. 21) and the experimental location of the bright CT state (Ref. 46). The figure assumes degenerate energies for the two B_2-symmetry $X+C$ ER states, and again for the $X+B$ ER pair. The vertical line indicates the ground-state geometry for Franck-Condon considerations.

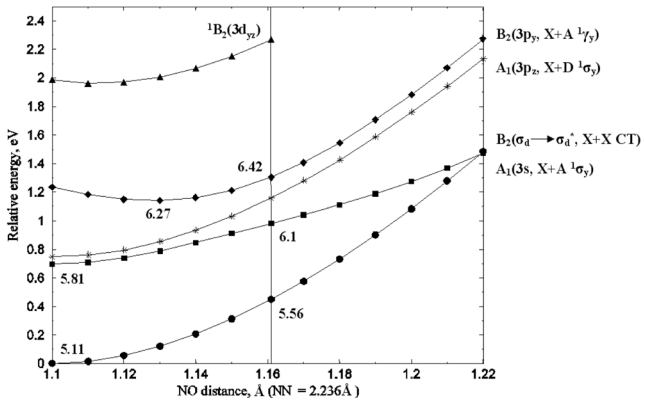

FIG. 10. EOM-EE-CCSD/6-311(2+)G(2df) results for selected dimer states, as a function of symmetric R(N–O) stretch. The R(N–N) and ∠ONN values were taken to be 2.236 Å and 99.6° (Ref. 42). The zero of energy corresponds to the "minimum" of the $^1A_1(3s)$ state. Vertical and "adiabatic" [with R(N–N) and ∠ ONN fixed] excitation energies are also shown. The characters of the $^1B_2$ states are inverted at smaller N–N distances due to an avoided crossing, similar to the crossing in Fig. 7.

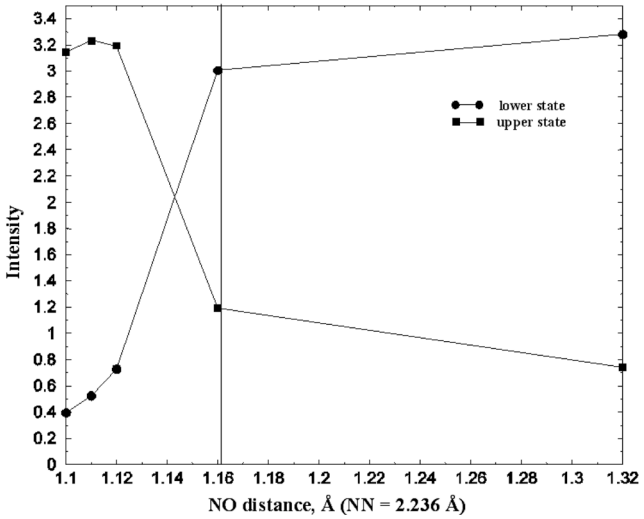

FIG. 11. The dependence of the absorption intensity $\langle\tilde{\mu}_{\mathrm{elec}}\rangle^2$ vs R(N–O) for the two B_2 transitions of mixed Rydberg ($3p_y$) and valence ($\sigma_d \rightarrow \sigma_d^*$) character, from the EOM-EE-CCSD runs of Fig. 10.

ymptotes could have large enough excimer splittings to come down into this energy region as well. The propensity of many B_2 states to borrow intensity from the CT state means that we cannot pinpoint all the adiabatic state(s) that are likely to be directly accessed upon UV light absorption. The large density of states and strong Rydberg-valence mixings suggest that more than one adiabatic state could be initially excited.

V. DISCUSSION

A. Computational aspects

The charge-transfer or charge-resonance state $CT_1(\sigma_d \rightarrow \sigma_d^*)$, with $7a_1^1 7b_2^1(\sigma_d^1 \sigma_d^{*1})$ occupation and $^1B_2$ symmetry, is the dominant absorbing state of $(NO)_2$ in the ultraviolet, as shown by Table II. This bright diabatic state lends intensity to several adiabatic states across an energy region of several eV, as shown by Table III. These results can explain the broad (5–7 eV) and featureless predissociative absorption band found experimentally:[46] the wide-ranging influence of CT_1 induces intensity borrowing by nearby excimer states, which have generally weak binding energies, and these states likely produce broad overlapping dissociative bands.

The oscillator strength (f value) for the overall band was determined to be 0.26.[46] We can derive *ab initio* f values by deriving squared transition moment values for the diabatic CT_1 state, and using the formula $f=(3.037\times10^{-6}\ \mathrm{cm})\ \nu(\mathrm{cm}^{-1})\ \langle\mu(\mathrm{a.u.})\rangle^2$ where $\nu=5\times10^4\ \mathrm{cm}^{-1}$. For EOM-EE-CCSD, we sum the intensities of the two lowest B_2 states in Table II and obtain $\mu^2=4.2$ a.u. and $f=0.6$. For CASSCF and MRCISD, we divide an adiabatic intensity from Table IV by the square of the coefficient of CT_1 contribution, and obtain $\mu^2=1.9$–2.0 a.u. and $f=0.3$ for CASSCF, and $\mu^2=2.6$–2.8 a.u. and $f=0.4$ for MRCISD. The predicted 0.3–0.6 range of values is probably an upper bound to the measured value of 0.26, and certainly close enough to make the assignment and confirm the strong nature of the absorption.

Table IV clearly demonstrates the difficulty in computing the vertical excitation energy of the adiabatic state that is predominantly CT_1, since the calculated energies vary significantly, from 9.68 to 6.08 eV. Our best estimate, EOM-EE-(2,3)/extrapolated, placed this state at 6.49 eV. The basis set extrapolation is probably the largest remaining cause of error, due to the significant Rydberg character of this state. Higher excitations might also be important, e.g., the triple and quadruple excitations were crucial in lowering the energy of NO^- enough to predict a bound monomer anion,[22] and it appears to be the reason why EOM-CC outperforms MRCISD for this dimer state. Further improvements may bring our prediction for the CT_1 state of $(NO)_2$ more in line with the 6.0 eV value from the experimental peak maximum. Overall, the EOM-EE-CCSD/6-311(2+)G(2*df*) method provided the most accurate CT_1 energy, and therefore we employed this method to get more realistic "cuts" of the relevant excited state potential energy surfaces.

The state catalog (Table I) predicts a large density of ultraviolet singlet states, and many have been verified with our CASSCF calculations (Fig. 6). Almost all excited states are predicted to be of multiconfigurational character, at dimer geometries and even more so at increased intermonomer distances, indicating strong nondynamical correlation effects. The origin of this nondynamical correlation and the high density of states is the quasidegeneracy of the four dimer orbitals derived from the four π^* orbitals of the NO monomers.[7] In addition, avoided crossings and intensity borrowing result in adiabatic states of mixed CT/Rydberg character, and our EOM-EE-CCSD calculations suggest a near-equal mixing of two B_2-symmetry states ($X+X\ CT_1$ and $X+A\ 3p_y$) in the region of 6 eV vertical excitation.

The tandem approach of single-reference EOM-CCSD and multireference approaches proved useful because the two techniques have complementary strengths. The EOM-CCSD calculations omit doubly excited configurations, which for this dimer might sacrifice some nondynamical correlation and predict limited intensity borrowing from CT_1, but they describe accurate Rydberg-valence interactions by predicting the energies of Rydberg and valence states with roughly equal accuracy. The MRCISD calculations have no nondynamical weaknesses and were useful in demonstrating trends with increased dynamical correlation, but for this dimer they failed to provide enough dynamical correlation for CT_1, leaving an imbalance in Rydberg and valence state descriptions. The CASSCF calculations, unsuitable for vertical excitation energies and quantitative state mixing, were ideal for the qualitative work in establishing the state catalog and correlations to monomer states, and investigating excimer splittings and the intensity-borrowing phenomenon.

More quantitative vertical excitation results are unattainable at this time. This difficult dimer has too many UV states and requires highly accurate treatment of both dynamical and nondynamical electron correlations. As with the infrared states, the UV states of the nitric oxide dimer are an excellent (and imposing!) test of electronic structure methods. We hope our comparative testing of multireference and EOM-CC methods here will prove useful in applications to other molecules. Nevertheless, the results presented here rep-

resent a large step forward in understanding the electronic structure of the NO dimer. Specifically, we can conclude the following on the basis of theory alone.

(i) There are numerous electronic states in the excitation region of 5–7 eV.
(ii) A single B_2-symmetry charge-transfer state, CT_1, lends "brightness" to several B_2 states, resulting in several adiabatic states of mixed valence (CT)-Rydberg character.
(iii) When the molecule absorbs a 6 eV photon, it enters a CT_1 diabatic state which is well bound ($-1/R$ attractive potential), and in order to dissociate into monomers it would need to evolve into energetically nearby and vibrationally excited Rydberg exciton states, which have low binding energies.
(iv) No single theoretical method can account for all the states and with correct energies; therefore, there is still some uncertainty regarding the vertical and adiabatic excitation energies, the composition of each state, and the variation of electronic configuration with the change of coordinates.

B. Ultraviolet photodissociation dynamics: Synergism between theory and experiment

In combining experimental results with the theory and computation results presented here, a picture now emerges that can successfully account for many experimental results in the UV wavelength region.

Photofragment spectra show that UV optical excitation accesses state(s) of B_2 symmetry throughout the 244–190 nm band, and photoelectron spectra indicate that removing an electron from the excited state results predominantly in dissociative ionization. The latter is typical of ionization of a state with geometry different than that of the ground state of the ion. Theory identifies the nature of the state with the largest oscillator strength as a predominantly CT_1 state in the Franck-Condon (FC) region. Furthermore, theory finds that CT states contribute to several adiabatic states of B_2 symmetry, the lowest being of dimer-$3p_y$ Rydberg character with an adiabatic dissociation asymptote at 5.45 eV to NO(X)+NO(A) products (Table I). The broad (5–7 eV) UV absorption band is almost featureless because the CT component dephases quickly; a structured absorption spectrum is generally expected for electronic states having electronic dephasing times longer than those of vibrational motions. In fact, had the dimer's 3s and 3p Rydberg states been absent or lie at higher energy, this CT state would most likely produce (contrary to what is observed) a structured absorption spectrum and a photoelectron spectrum with short and distinct vibrational progressions,[47] because the preferred geometries of ground-state $(NO)_2$, the diabatic CT_1 state, and the $(NO)_2^+$ ground state are similar.

We believe that the coupling of CT_1 with Rydberg and valence states that correlate asymptotically with Rydberg (A) or valence (B) states of the product is responsible for ionization into the dissociative states of the ground state ion. In particular, at 6 eV, the NO stretch vibrational progression presented in Paper II suggests that the intermediate state here prefers a geometrical displacement along the NO stretch coordinate. Our EOM-EE-CCSD results support this notion, predicting R(N–O) contraction (Fig. 10) due to the avoided crossing with an $X+A$ $3p_y$ Rydberg state.

At still higher energies, e.g., when the $X+A$, $X+B$, $X+C$, and $X+D$ channels are all open, several excited states may be accessed coherently via their CT components (Fig. 9). The nonstationary "bright" state then may dephase to stationary states of mixed Rydberg/CT or valence/CT character, accounting for the simultaneous production of several final channels, as observed experimentally. For example, Naitoh *et al.*[48] observed NO in both Rydberg (A) and valence (B) states at 193 nm, whereas Dribinski *et al.*[15] identified NO in Rydberg (A, C, and D) and valence (B) states in two-photon excitation experiments at 160–180 nm (7–8 eV).

At longer wavelengths, just above and below the $X+A$ threshold, the bright state is the CT_1 diabatic state, and we place the origin of the lowest B_2/CT_1 state below the $X+A$ threshold, at 5.12 eV, in agreement with resonantly enhanced multiphoton ionization (REMPI) experiments [to be discussed in II (Ref. 2) and III (Ref. 3)]. The $A_1(3s)$ state does not have CT_1 character and is not accessed optically because of its small oscillator strength. We note, however, that it may be accessed from the B_2 state by a conical intersection promoted by any nonsymmetric vibration that gives the dimer an instantaneous $C_s(A')$ character. Experimental results in II and III suggest, however, that such intersections—if they exist—must occur far from the Franck-Condon region, most likely in the exit valley.

Now we specifically address 210–200 nm (~6 eV) excitation, i.e., near the peak of the absorption curve, as in Papers II and III of this series. Experimentally, once the UV photon is absorbed, the dimer dissociates in a time scale of several hundred femtoseconds. Theory says that since the diabatic CT_1 state has a rising $-1/R$ potential that prevents the dimer from dissociating diabatically at 6 eV, clearly the molecules which access this state must evolve into a continuum level of a Rydberg or valence state in order to dissociate. The similar energies of Rydberg dimer and valence states correlating with $X+A$ and $X+B$ states provide such a route, and the combined results of II, III, and theory all self-consistently suggest that the dimer $3p_y$ Rydberg orbital is involved in the dissociation. We have shown in Table I that such a state must correlate with $X+A$ via an out-of-phase orbital combination of the monomer's occupied 3s Rydberg orbital. At times longer than 1 ps after pump photon absorption, the ejected electron is typical of ionization of an NO(A) Rydberg product state. What is unclear from either experiment or theory is whether the state evolution is via nonadiabatic coupling, adiabatic dephasing, or both.

To discuss the state evolution we now examine in more detail the picture described by EOM-EE-CCSD in Figs. 7 and 10. Initial absorption excites the molecules vertically to a vibrationally excited state of one of the two B_2-symmetry electronic states, as shown in the figures. The best Franck-Condon factors appear to be for states of low quanta in ν_3 (intermonomer stretch, Fig. 7), two to four quanta in ν_1 (N–O symmetric stretch, Fig. 10), and unknown quanta in

the other modes. This would result in the excited molecule initially undergoing $R(\mathrm{N-O})$ vibration that causes the excited electronic state to oscillate every ~20 fs, between electronic configurations that are CT-like at the outer $R(\mathrm{N-O})$ and $3p_y$ Rydberg type at the inner $R(\mathrm{N-O})$ classical turning points. From here, we can envision two plausible scenarios. In a purely adiabatic mechanism, vibrational mode coupling allows intramolecular vibrational energy redistribution (IVR) that transforms ν_1 $R(\mathrm{N-O})$ stretching into ν_3 intermonomer stretching (and other low frequency modes) in two discernible stages. There might be a 140 fs time scale in which the electronic state has lost its oscillating CT_1 character, due to the loss via IVR of sufficient ν_1 stretch quanta to restrict the $R(\mathrm{N-O})$ to smaller, more Rydberg-type ranges. Then, on a 590 fs time scale, the remaining ν_1 stretch quanta could be lost via IVR, providing enough energy in the ν_3 direction to dissociate. This scenario would explain both the lack of structure in the absorption spectrum and the dominance of dissociative ionization in the photoelectron spectrum. In a second mechanism, via nonadiabatic coupling, the molecule may instead undergo mode-assisted internal conversion, via a_1-symmetry vibrations, to a vibronic level of the other B_2-symmetry electronic state, on a 140 fs time scale. Then, on a 590 fs time scale, it would convert its ν_1 quanta to ν_3 via IVR in order to dissociate. The small uncertainties in the computed state energies, and the many dynamical possibilities (e.g., conical intersections with Rydberg states of other symmetries), make this level of detail in the 6 eV photodissociation mechanism somewhat speculative; finer details of the dissociation mechanism cannot be completely elucidated at present.

VI. SUMMARY

Molecular orbital theory and calculations were used to describe the ultraviolet singlet excited states of NO dimer. Qualitatively, we derived and cataloged the dimer states by correlating them with monomer states, and provided illustrative CASSCF calculations. Quantitatively, we provide computational estimates of vertical transition energies and absorption intensities with MRCI and EOM-CC methods. We have identified a bright charge-transfer (charge-resonance) state as responsible for the broadband seen in UV absorption experiments, but its vertical excitation energy was difficult to reproduce due to hefty amounts of dynamical correlation in the state. EOM-EE-CCSD was able to reproduce this energy best, and it allowed the observation of an important avoided crossing between this state and a Rydberg state that is dimer $3p_y$ in character, but dissociates to $X+A$ monomers where the A state is monomer $3s$ in character.

Both our state catalog and our EOM-EE-CCSD results were used, in synergy with past and present experimental results, to elucidate the interesting UV photophysics of this dimer. The unexpected tendency of probe photons to result in dissociative ionization was explained by Rydberg-CT coupling, which causes the $R(\mathrm{N-O})$ distorted nature of the initially pumped state. General observations of various dissociative thresholds (to $X+A$, $X+B$, etc.) were discussed and explained. Finally, the two-step mechanism observed in our time-resolved 6 eV photodissociation experiments,[1] detailed in the next two Papers II and III of this series,[2,3] is interpreted as an initial evolution from a bound CT diabatic state to the $3p_y$ Rydberg state (both of B_2 symmetry), and a further evolution of the dimer $3p_y$ Rydberg state to a final monomer-$3s$ Rydberg product state. Finer details must await further study.

ACKNOWLEDGMENTS

Funding is acknowledged from the Natural Sciences and Engineering Research Council of Canada (A.U.E. and A.S.), the Canada Foundation for Innovation (A.L.L.E.), and the National Science Foundation (H.R. and A.I.K.). Several scientists are thanked for valuable discussions: K. P. Huber, J. K. G. Watson, C. C. Hayden, J. G. Underwood, and A. M. D. Lee.

[1] O. Gessner, A. M. D. Lee, J. P. Shaffer *et al.*, Science **311**, 219 (2006).
[2] O. Gessner, A. M. D. Lee, H. Reisler, *et al.* (unpublished).
[3] O. Gessner A. M. D. Lee, H. Reisler, *et al.* (unpublished).
[4] E. A. Wade, J. I. Cline, K. T. Lorenz, C. Hayden, and D. W. Chandler, J. Chem. Phys. **116**, 4755 (2002).
[5] R. Hetzler, M. P. Casassa, and D. S. King, J. Phys. Chem. **95**, 8086 (1991).
[6] A. B. Potter, V. Dribinski, A. V. Demyanenko, and H. Reisler, J. Chem. Phys. **119**, 7197 (2003).
[7] A. R. W. McKellar, J. K. G. Watson, and B. J. Howard, Mol. Phys. **86**, 273 (1995).
[8] C. M. Western, P. R. R. Langridge-Smith, B. J. Howard, and S. E. Novick, Mol. Phys. **44**, 145 (1981).
[9] Y. Matsumoto, Y. Ohshima, and M. Takami, J. Chem. Phys. **92**, 937 (1990).
[10] A. L. L. East, J. Chem. Phys. **109**, 2185 (1998).
[11] R. Sayos, R. Valero, J. M. Anglada, and M. Gonzalez, J. Chem. Phys. **112**, 6608 (2000).
[12] M. Tobita, S. A. Perera, M. Musial, R. J. Bartlett, M. Nooijen, and J. S. Lee, J. Chem. Phys. **119**, 10713 (2003).
[13] A. V. Demyanenko, A. B. Potter, V. Dribinski, and H. Reisler, J. Chem. Phys. **117**, 2568 (2002).
[14] V. Dribinski, A. B. Potter, I. Fedorov, and H. Reisler, Chem. Phys. Lett. **385**, 233 (2004).
[15] V. Dribinski, A. B. Potter, I. Fedorov, and H. Reisler, J. Chem. Phys. **121**, 12353 (2004).
[16] A. B. Potter, J. Wei, and H. Reisler, J. Phys. Chem. B **109**, 8407 (2005).
[17] V. Blanchet and A. Stolow, J. Chem. Phys. **108**, 4371 (1998).
[18] A. Stolow, Annu. Rev. Phys. Chem. **54**, 89 (2003); A. Stolow, A. E. Bragg, and D. M. Newmark, Chem. Rev. (Washington, D.C.) **104**, 1719 (2004).
[19] M. Tsubouchi, C. A. de Lange, and T. Suzuki, J. Chem. Phys. **119**, 11728 (2003).
[20] M. Tsubouchi and T. Suzuki, Chem. Phys. Lett. **382**, 418 (2003).
[21] R. de Vivie and S. D. Peyerimhoff, J. Chem. Phys. **89**, 3028 (1988).
[22] R. Polák and J. Fišer, Chem. Phys. **303**, 73 (2004).
[23] E. S. Chen, W. E. Wentworth, and E. C. M. Chen, J. Mol. Struct. **606**, 1 (2002).
[24] A. L. L. East and E. C. Lim, J. Chem. Phys. **113**, 8981 (2000).
[25] K. P. Huber and G. Herzberg, *Constants of Diatomic Molecules* (Van Nostrand, New York, 1979).
[26] H.-J. Werner, P. J. Knowles, M. Schütz *et al.*, MOLPRO 2002.6 is a package of *ab initio* programs.
[27] H.-J. Werner and P. J. Knowles, J. Chem. Phys. **82**, 5053 (1985).
[28] P. J. Knowles and H.-J. Werner, Chem. Phys. Lett. **115**, 259 (1985).
[29] H.-J. Werner and P. J. Knowles, J. Chem. Phys. **89**, 5803 (1988).
[30] P. J. Knowles and H.-J. Werner, Chem. Phys. Lett. **145**, 514 (1988).
[31] J. Kong, C. A. White, A. I. Krylov *et al.*, J. Comput. Chem. **21**, 1532 (2000).
[32] J. F. Stanton, J. Gauss, J. D. Watts *et al.*, ACES II is a program product of the Quantum Theory Project, University of Florida; Integral packages included are VMOL (J. Almlöf and P. R. Taylor); VPROPS (P. Taylor);

ABACUS (T. Helgaker, H. J. Aa. Jensen, P. Jørgensen, J. Olsen, and P. R. Taylor).
[33] J. F. Stanton and R. J. Bartlett, J. Chem. Phys. **98**, 7029 (1993).
[34] S. V. Levchenko and A. I. Krylov, J. Chem. Phys. **120**, 175 (2004).
[35] L. V. Slipchenko and A. I. Krylov, J. Chem. Phys. **123**, 084107 (2005).
[36] S. Hirata, M. Nooijen, and R. J. Bartlett, Chem. Phys. Lett. **326**, 255 (2000).
[37] As an example, for singlet states of the CH_2 diradical, EOM-EE-CCSD calculations based on a closed-shell singlet reference configuration gave superb results for the singly excited $\tilde{a}\,^1A_1$-$\tilde{b}\,^1B_2$ gap (0.03 eV error relative to full CI), but expectedly poor results for the doubly excited $\tilde{a}\,^1A_1$ -$\tilde{c}\,^1A_1$ gap (1.1 eV error relative to full CI); [L. V. Slipchenko and A. I. Krylov, J. Chem. Phys. **117**, 4694 (2002)].
[38] E. D. Glendening, J. K. Badenhoop, A. E. Reed, J. E. Carpenter, J. A. Bohmann, C. M. Morales, and F. Weinhold, NBO 5.0, Theoretical Chemistry Institute, University of Wisconsin, Madison, WI, 2001.
[39] R. A. Kendall, T. H. Dunning, Jr., and R. J. Harrison, J. Chem. Phys. **96**, 6796 (1992).
[40] R. Krishnan, J. S. Binkley, R. Seeger, and J. A. Pople, J. Chem. Phys. **72**, 650 (1980); M. J. Frisch, J. A. Pople, and J. S. Binkley, *ibid.* **80**, 3265 (1984).
[41] P. C. Hariharan and J. A. Pople, Theor. Chim. Acta **28**, 213 (1973). Diffuse exponents: T. Clark, J. Chandrasekhar, and P. v. R. Schleyer, J. Comput. Chem. **4**, 294 (1983).
[42] S. G. Kukolich, J. Mol. Spectrosc. **98**, 80 (1983).
[43] R. S. Mulliken, J. Chem. Phys. **7**, 20 (1939).
[44] J. S. Sears, C. D. Sherrill, and A. I. Krylov, J. Chem. Phys. **118**, 9084 (2003).
[45] A. Tajti, P. G. Szalay, A. G. Császár, M. Kállay, J. Gauss, E. F. Valeev, B. A. Flowers, J. Vázquez, and J. F. Stanton, J. Chem. Phys. **121**, 11599 (2004).
[46] J. Billingsley and A. B. Callear, Trans. Faraday Soc. **67**, 589 (1971).
[47] A. Strobel, N. Knoblauch, J. Agreiter, A. M. Smith, G. Niedner-Schatteburg, and V. E. Bondybey, J. Phys. Chem. **99**, 872 (1995).
[48] Y. Naitoh, Y. Fujimura, K. Honma, and O. Kajimoto, J. Phys. Chem. **99**, 13652 (1995).